Optics Letters

High conversion efficiency second-harmonic beam shaping via amplitude-type nonlinear photonic crystals

Bing Zhu,† Haigang Liu,† Yuping Chen,* and Xianfeng Chen

State Key Laboratory of Advanced Optical Communication Systems and Networks, School of Physics and Astronomy, Shanghai Jiao Tong University, 800 Dongchuan Road, Shanghai 200240, China
**Corresponding author: ypchen@sjtu.edu.cn*

Received 31 October 2019; revised 20 November 2019; accepted 20 November 2019; posted 20 November 2019 (Doc. ID 382108); published 24 December 2019

An efficient two-dimensional arbitrary harmonic wavefront shaping has been demonstrated in amplitude-type nonlinear photonic crystals, where the phase-matching condition is fulfilled through the birefringence and nonlinear Raman–Nath effects in longitudinal and transverse phase matching, respectively. The binary modulated nonlinear photonic crystal was fabricated by femtosecond laser micromachining based on binary computer-generated holograms. Three second-harmonic Hermite–Gaussian beams, HG_{10}, HG_{11}, and HG_{12}, were achieved by pumping a nanosecond pulsed fundamental Gaussian beam, with the measured normalized conversion efficiency of 8.4%W^{-1} cm^{-2} in the first diffraction order of the HG_{11} structure. The amplitude-type nonlinear photonic crystal opens wide possibilities in the field of efficient harmonic beam shaping and mode conversion.

https://doi.org/10.1364/OL.45.000220

Nonlinear frequency conversion in quadratic nonlinear crystals is an important method to generate coherent radiation in wavelengths when compact and efficient sources are not available [1,2]. It is worth noting that beam shaping of a nonlinear harmonic wave has attracted intense interest in recent years and has been studied in various applications [3,4], including optical micro-manipulation [5–7], optical micro-fabrication [8], optical imaging [9,10], quantum optics [11–14], and optical communication [15–17]. The usual way to realize the beam shaping of a nonlinear harmonic wave is to generate a beam in the nonlinear crystal first and shape the beam in the next step with filters, lenses, mode converters, spatial light modulators, or other conventional optical elements placed beyond the exit facet of the nonlinear crystal. However, these optical elements often consume a large workspace while increasing the mechanical stability requirement of the whole system [18]. A novel method for overcoming these problems is to integrate the beam-shaping process within the nonlinear optical microstructured materials, such as nonlinear photonic crystals (NPCs) [19–21] and nonlinear metamaterials [22,23]. To achieve the desired beam profile in NPCs, the electric-field poling technique has been used to spatially modulate the second-order nonlinear coefficient of the crystal. The beam profile can be manipulated to realize beam shaping [24–26], focusing [27], and steering [28]. However, this approach is challenging in achieving efficient nonlinear harmonic frequency along with the shaping of the beam in two transverse dimensions, since the longitudinal part of the vectorial phase-matching condition is not fulfilled.

In this Letter, we demonstrate efficient two-dimensional (2D) arbitrary harmonic beam shaping, with three Hermite–Gaussian (HG) beams, HG_{10}, HG_{11}, and HG_{12}, in the second-harmonic (SH) beam with measured normalized conversion efficiency of 8.4%W^{-1} cm^{-2} achieved in the quadratic nonlinear crystal. We named these crystals as amplitude-type NPCs (A-NPCs). The A-NPCs are fabricated by femtosecond laser micromachining and have a geometric specific pattern with 0 or +1 binary modulation of quadratic susceptibility in ferroelectric crystals designed by computer-generated holograms (CGHs). The modulated NPC was cut for a specific angle between the optical axis and the z axis of the crystal, where the phase-matching condition is fulfilled through birefringence phase matching (BPM) and the nonlinear Raman–Nath process in longitudinal and transverse, respectively.

A standard method for 2D beam shaping in linear optics is based on the use of CGH [29]. When sending a light beam through a CGH pattern, the far-field diffracted wavefront will have the desired amplitude and phase. Several methods of implementing the coding of information in a CGH have been developed, e.g., encoding in a continuous [30] or a binary [31] form. Since the A-NPCs use the nonlinear Raman–Nath process [32] to fulfill the transverse part of the vectorial phase-matching condition, we cannot use a coding function that relies on continuous modulation of the amplitude and phase. Then the only possibilities we have are either an entirely positive or an erased zero quadratic susceptibility throughout the interaction region by femtosecond micromachining. Fortunately, such a case of binary modulation has already been addressed in the field of linear CGH by Lee [31], who suggested the following binary coding method for the amplitude transmittance function of a CGH:

$$t(x,y)=\begin{cases}1 & \cos[2\pi f_{\text{carrier}}x-\varphi(x,y)]-\cos[\pi q(x,y)]\geq 0,\\ 0 & \text{otherwise,}\end{cases} \tag{1}$$

where $q(x,y)$ is the function of the amplitude of the encoded information, defined by $\sin[\pi * q(x,y)]=A(x,y)$. $A(x,y)$ is the amplitude of the Fourier transform (FT) of the desired wavefront in the first diffraction order, which is normalized to the range of 0–1. $\varphi(x,y)$ is the phase of the FT of the desired wavefront in the first diffraction order, which is in the range of $0-2\pi$. Also, $q(x,y)$ is in the range of 0–0.5; f_{carrier} represents the frequency of the carrier function. We can use this function to realize a 2D nonlinear CGH in A-NPCs. The 2D modulation of the second-order nonlinearity coefficient of an A-NPC in this case is

$$d_{\text{NLO}}(x,y)=\tfrac{1}{2}d_{ij}\{1+\text{sign}\{\cos[2\pi f_{\text{carrier}}x-\varphi(x,y)]-\cos[\pi q(x,y)]\}\}, \tag{2}$$

where d_{ij} represents an element of the quadratic nonlinear susceptibility $\chi^{(2)}$ tensor. Without regard to the amplitude or phase modulation of the beam shaping, the nonlinear coefficient of the structure is periodically modulated by the angular frequency $2\pi f_{\text{carrier}}$. In this case, the nonlinear Raman–Nath process generates an SH beam at the angle $\theta_{\text{RN}}=\arcsin(2\pi f_{\text{carrier}}/k_{2\omega})$, which is equivalent to the angle of the first diffraction order in the case of a regular grating with the same angular frequency. When the amplitude and the phase are added, the far-field SH beam profile at this first diffraction order is the FT of $A(x,y)\exp[i\phi(x,y)]$ [25]. What needs to be pointed out is that the nonlinear Raman–Nath process provides only the transverse matching of the wave vectors; the longitudinal part of the vectorial phase-matching condition is fulfilled by the BPM process, which will be illustrated later in this Letter.

To demonstrate the concept of A-NPCs, we chose to fabricate a crystal aimed to generate three modes from the HG family, HG_{10}, HG_{11}, and HG_{12}, in the first diffraction order. The transverse spatial distribution of the HG modes at origin is

$$U_{l,m}(x,y,0)=A_{l,m}G_l\left[\frac{\sqrt{2}x}{W_0}\right]G_m\left[\frac{\sqrt{2}y}{W_0}\right], \tag{3}$$

where $A_{l,m}$ represents the amplitude, W_0 is the waist, and $G_l(u)$ represents the lth-order HG function.

Different from the previous method of using electric-field poling to produce the NPCs, femtosecond laser micromachining is used to fabricate the A-NPCs in this Letter. In recent research, the femtosecond laser has been proven a convenient technique to invert [33,34] or erase [35,36] second-order nonlinear susceptibility. A schematic illustration of the fabrication process of the A-NPCs by femtosecond laser micromachining is shown in Fig. 1(a), with the CGH pattern of HG_{11} structure embedded in the nonlinear crystal. We fabricated the suggested structure in a 5 mol. % MgO-doped lithium niobate ($LiNbO_3$) crystal with dimensions of 10 mm (x) ×10 mm (y) ×1 mm (z). In addition, the $LiNbO_3$ was cut for a specific angle of $\theta=75°$ between the optical axis (c axis) and the z axis of the crystal. A compact ytterbium-doped diode-pumped ultrafast amplified laser was employed as a laser source, which delivered linearly polarized pulses with a duration of 500 fs (FWHM), a center wavelength at 1030 nm, and a repetition rate of 1 kHz. An objective lens with a numerical aperture of 0.50 (RMS20X-PF, Olympus) was applied to focus the laser pulses. The crystal sample was mounted on a computer-controlled XYZ translation piezo-stage with 0.1 μm resolution. To record the desired CGH pattern in A-NPC, the crystal sample was moved step by step and irradiated by the focused femtosecond laser pulses according to the specific hologram pattern. The irradiated dots became "black" by selectively erasing the ferroelectric domain with femtosecond laser pulses, while the unirradiated dots remained "blue." A magnified illustration of the geometric specific pattern with 0 or +1 binary modulation of the quadratic nonlinear susceptibility $\chi^{(2)}$ in $LiNbO_3$ is shown in Fig. 1(b). The physical mechanism of the ferroelectric domain erasing process can be understood in that the crystallinity is reduced through laser irradiation, which has been verified by measurements of the transmission electron microscopy (TEM) diffraction pattern and micro-Raman signal in the engineered area by Wei *et al.* [35] in previous research work.

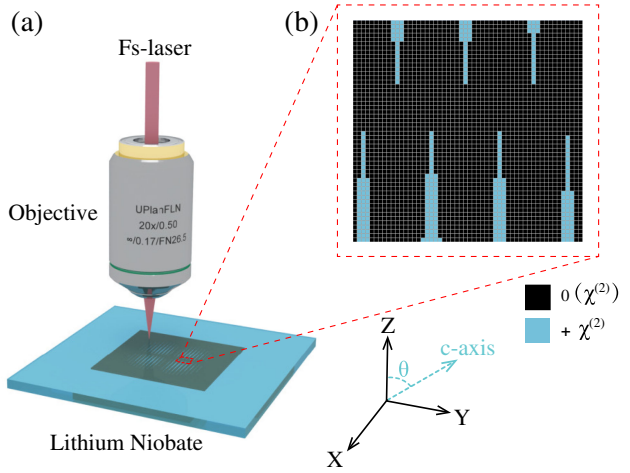

Fig. 1. (a) Schematic illustration of the A-NPCs by femtosecond laser micromachining for the HG_{11} structure and (b) the geometric specific pattern with 0 or +1 binary modulation of the quadratic nonlinear susceptibility $\chi^{(2)}$ in lithium niobate. The crystal was cut for a specific angle between the c axis and z axis.

We fabricated the specific pattern with 512 × 512 pixels, where each pixel is approximately 2 μm × 2 μm by the scanning process of the femtosecond laser pulses. The chirped pulses were focused 30 μm beneath the front surface of the sample with the incident energy of 0.9 μJ per pulse. The CGH was first scanned in x direction step by step and then moved to the next pixel by moving in $+y$ direction. The odd pixels and even pixels were all scanned in the same $+x$ direction. The translation speed was 280 μm/s. The final fabricated crystal had three separate $\sim 1.0\times 1.0\ \text{mm}^2$ structures, with different modulations of the quadratic nonlinear susceptibility $\chi^{(2)}$, according to Eq. (2). Figure 2 shows a comparison between the calculated, fabricated, and SH image of the CGH patterns in the HG_{10}, HG_{11}, and HG_{12} structures, respectively. Figures 2(d)–2(f) are the microscope pictures of the $x-y$ surface of the crystal after femtosecond micromachining, and the excellent quality of the fabrication process can be observed. Also, the SH image of the CGH patterns shown in Figs. 2(g)–2(i) are in good agreement with the calculated and fabricated patterns.

A schematic illustration of the proposed experimental nonlinear wavefront shaping setup using A-NPC is shown in Fig. 3.

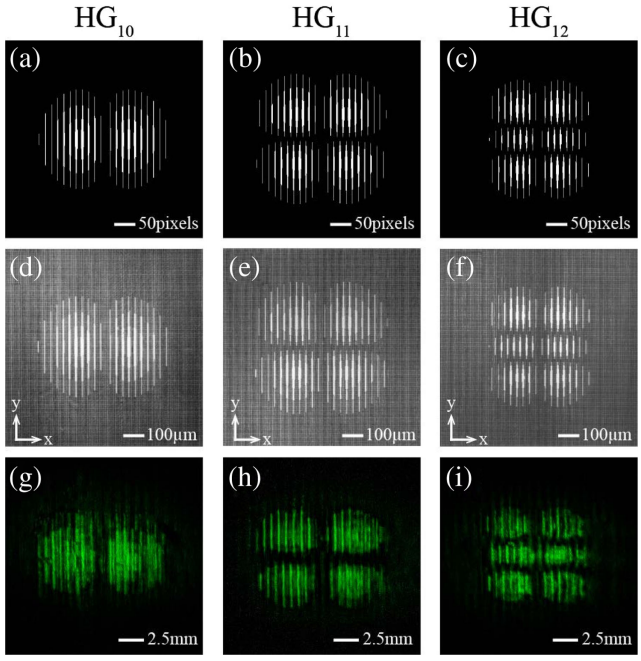

Fig. 2. Comparison between (a)–(c) calculated, (d)–(f) fabricated, and (g)–(i) SH image of the CGH patterns in the HG_{10}, HG_{11}, and HG_{12} structures, respectively.

We used an Nd:YAG laser producing 10.5 ns pulses at a 1 kHz repetition rate at a wavelength of 1064 nm as the fundamental frequency (FF) source. An ordinary polarized laser beam was irradiated on the center of the CGH pattern in the crystal, creating a waist radius of approximately 500 μm, and generated an extraordinary polarized SH beam at the wavelength of 532 nm. The polarization axis of the incident ordinary polarized fundamental wave was parallel to the x direction. A filter (TF1, Thorlabs) was used to separate the FF and SH beams. Also, the illustration shows the fabrication pattern of the crystal computed for HG_{11} and the transverse setting in which the experiment took place. Numerical simulation was performed on a screen in the far field based on the split-step Fourier method. The A-NPC was cut for the type I (oo-e) phase-matching process based on the BPM [37] theory of the $LiNbO_3$ crystal. Hence, the longitudinal part of the vectorial phase-matching condition was fulfilled. In addition, the transverse part of the vectorial phase-matching condition was fulfilled through the nonlinear Raman–Nath process. Because of the full matching of the wave vectors, efficient nonlinear harmonic wavefront shaping can be obtained in the first diffraction order in the far field.

We obtained desired HG modes at the first (left and right, −1 and +1) diffraction order. The frequency of modulation in the y direction, f_{carrier}, was chosen to be 0.04 μm^{-1}; therefore, the first diffraction order was obtained at an external angle of $\lambda_{SH} f_{\text{carrier}} \sim 21.3$ mrad, where λ_{SH} is the SH wavelength. Figure 4 presents the comparison between theoretical and measured beam profiles at the first diffraction order in the HG_{10}, HG_{11}, and HG_{12} structures, respectively. The results show high correlation values between theoretical predictions and experiments of the generated HG beams: HG_{10}(93%), HG_{11}(92%), and HG_{12}(92%) [38].

We examined both the total SH generation power and the first diffraction order power of the HG_{11} structure in Fig. 5.

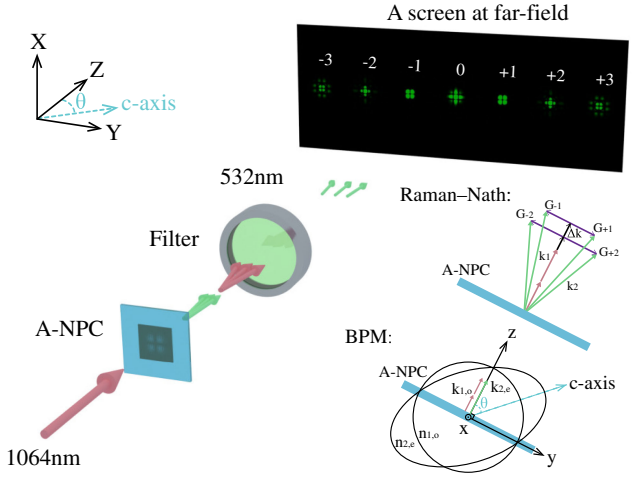

Fig. 3. Schematic illustration of the nonlinear wavefront shaping setup in A-NPC pumped by Nd:YAG laser with 10.5 ns pulse duration at a 1 kHz repetition rate at 1064 nm. The screen in the far field is the simulation result for HG_{11}. The bottom right is the schematic illustration of the fulfilled phase-matching condition through the BPM and nonlinear Raman–Nath process in longitudinal and transverse, respectively, where $\vec{k}_1$ represents the wave vector of the FF beam and $\vec{k}_2$ represents the wave vector of the SH beam. Subscripts "o" and "e" represent the ordinary and extraordinary polarized light, respectively, and $\vec{G}_m$ represents the transverse reciprocal vector in the mth diffraction order of the SH wave. The Δk is the momentum mismatch in the propagation directions for various diffraction orders of the nonlinear Raman–Nath diffraction.

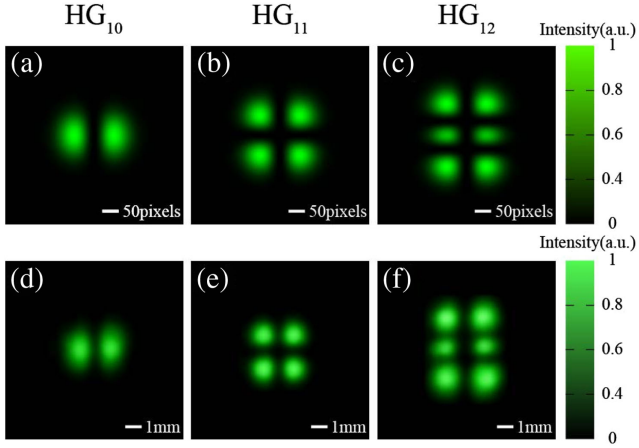

Fig. 4. Comparison between (a)–(c) theoretical and (d)–(f) measured beam profiles at the first diffraction order in the HG_{10}, HG_{11}, and HG_{12} structures, respectively.

These plots confirm a well-known fundamental quadratic relation between intensity of the SH and fundamental beams. The fair agreement between the values indicates that the A-NPC structures are sufficient for the realization of highly efficient 2D harmonic beam shaping. The measured normalized conversion efficiency η_{nor} can be calculated by

$$\eta_{\text{nor}} = \frac{P_{2\omega}}{P_{\omega}^{2} \cdot L^{2}}, \tag{4}$$

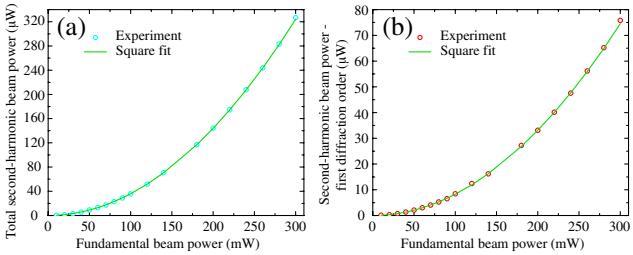

Fig. 5. Comparison between measured (circle) and square fit (solid curves) results: (a) total SH output power dependence on FF input power and (b) first diffraction order SH output power dependence on FF input power.

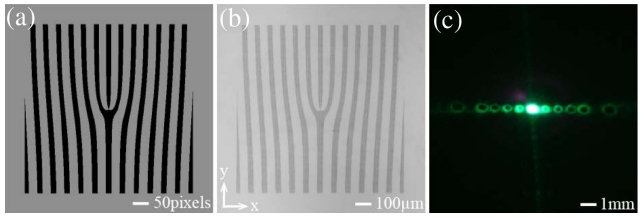

Fig. 6. (a) Calculated, (b) fabricated, and (c) far-field experiment result of the fork grating structure for generating the nonlinear vortex beams.

where P_ω and $P_{2\omega}$ are the powers of the fundamental and harmonic, respectively, and L is the length over which the light beams propagate in the crystal [39]. The normalized conversion efficiency of HG_{11} structure in the +1 first diffraction order we calculated is $8.4\%W^{-1}\ cm^{-2}$, with the input power of 300 mW and SH power of 75.8 μW in the A-NPC of 1 mm thickness.

The A-NPCs can be used to generate arbitrary profiles of beams and are not limited to HG beams. We also demonstrate the generation of nonlinear vortex beams with the fork grating structure in A-NPC in Fig. 6.

In conclusion, we have proposed and realized efficient phase-matched nonlinear 2D beam shaping in A-NPCs fabricated by femtosecond laser micromachining. The approach can be utilized in different materials with different diffraction periods at broadband wavelengths. Furthermore, highly efficient nonlinear optical beam shaping can be employed for the desired wavefront and provide full control of the amplitude and the phase of the converted beam. The ability to convert the frequency of light and to reshape its wavefront simultaneously in the desired way will be useful for all-optical shaping, routing, and switching of beams.

Funding. National Natural Science Foundation of China (11574208, 91950107); National Key R & D Program of China (2017YFA0303700).

Acknowledgment. H. L. conceived ideas and guided the completion of the experiments. B. Z. fabricated structures and conducted frequency doubling experiments.

Disclosures. The authors declare no conflicts of interest.

†These authors contributed equally to this Letter.

REFERENCES

1. P. A. Franken, A. E. Hill, C. W. Peters, and G. Weinreich, Phys. Rev. Lett. **7**, 118 (1961).
2. J. A. Armstrong, N. Bloembergen, J. Ducuing, and P. S. Pershan, Phys. Rev. **127**, 1918 (1962).
3. H. Liu and X. Chen, J. Nonlinear Opt. Phys. Mater. **27**, 1850047 (2018).
4. S. Trajtenebrg-Mills and A. Arie, Opt. Mater. Express **7**, 2928 (2017).
5. J. Ng, Z. Lin, and C. T. Chan, Phys. Rev. Lett. **104**, 103601 (2010).
6. K. T. Gahagan and G. A. Swartzlander, J. Opt. Soc. Am. B **16**, 533 (1999).
7. S. H. Tao, X.-C. Yuan, J. Lin, X. Peng, and H. B. Niu, Opt. Express **13**, 7726 (2005).
8. M. Meier, V. Romano, and T. Feurer, Appl. Phys. A **86**, 329 (2007).
9. J. Chu, X. Li, Q. Smithwick, and D. Chu, Opt. Lett. **41**, 1490 (2016).
10. M. K. Sharma, J. Joseph, and P. Senthilkumaran, Appl. Opt. **50**, 5279 (2011).
11. A. Vaziri, J. Pan, T. Jennewein, G. Weihs, and A. Zeilinger, Phys. Rev. Lett. **91**, 227902 (2003).
12. J. Leach, B. Jack, J. Romero, M. Ritschmarte, R. W. Boyd, A. K. Jha, S. M. Barnett, S. Frankearnold, and M. J. Padgett, Opt. Express **17**, 8287 (2009).
13. R. Fickler, R. Lapkiewicz, W. N. Plick, M. Krenn, C. Schaeff, S. Ramelow, and A. Zeilinger, Science **338**, 640 (2012).
14. M. Malik, M. Erhard, M. Huber, M. Krenn, R. Fickler, and A. Zeilinger, Nat. Photonics **10**, 248 (2016).
15. J. Wang, J. Yang, I. Fazal, N. Ahmed, Y. Yan, H. Huang, Y. Ren, Y. Yue, S. Dolinar, M. Tur, and A. E. Willner, Nat. Photonics **6**, 488 (2012).
16. G. Milione, M. P. J. Lavery, H. Huang, Y. Ren, G. Xie, T. A. Nguyen, E. Karimi, L. Marrucci, D. A. Nolan, R. R. Alfano, and A. E. Willner, Opt. Lett. **40**, 1980 (2015).
17. Y. Zhao and J. Wang, Opt. Lett. **40**, 4843 (2015).
18. D. Singh, R. Shiloh, and A. Arie, Opt. Mater. Express **8**, 2654 (2018).
19. V. Berger, Phys. Rev. Lett. **81**, 4136 (1998).
20. N. G. R. Broderick, G. W. Ross, H. L. Offerhaus, D. J. Richardson, and D. C. Hanna, Phys. Rev. Lett. **84**, 4345 (2000).
21. A. Arie and N. Voloch, Laser Photon. Rev. **4**, 355 (2010).
22. N. Segal, S. Kerenzur, N. Hendler, and T. Ellenbogen, Nat. Photonics **9**, 180 (2015).
23. L. Wang, S. Kruk, K. L. Koshelev, I. I. Kravchenko, B. Lutherdavies, and Y. S. Kivshar, Nano Lett. **18**, 3978 (2018).
24. T. Ellenbogen, N. Volochbloch, A. Gananypadowicz, and A. Arie, Nat. Photonics **3**, 395 (2009).
25. A. Shapira, R. Shiloh, I. Juwiler, and A. Arie, Opt. Lett. **37**, 2136 (2012).
26. S. Trajtenberg-Mills, I. Juwiler, and A. Arie, Optica **4**, 153 (2017).
27. Y. Qin, C. Zhang, Y. Zhu, X. Hu, and G. Zhao, Phys. Rev. Lett. **100**, 063902 (2008).
28. T. Ellenbogen, A. Gananypadowicz, and A. Arie, Opt. Express **16**, 3077 (2008).
29. B. R. Brown and A. W. Lohmann, Appl. Opt. **5**, 967 (1966).
30. J. J. Burch, Proc. IEEE **55**, 599 (1967).
31. W. Lee, Appl. Opt. **18**, 3661 (1979).
32. S. M. Saltiel, D. N. Neshev, W. Krolikowski, A. Arie, O. Bang, and Y. S. Kivshar, Opt. Lett. **34**, 848 (2009).
33. T. Xu, K. Switkowski, X. Chen, S. Liu, K. Koynov, H. Yu, H. Zhang, J. Wang, Y. Sheng, and W. Krolikowski, Nat. Photonics **12**, 591 (2018).
34. S. Liu, K. Switkowski, C. Xu, J. Tian, B. Wang, P. Lu, W. Krolikowski, and Y. Sheng, Nat. Commun. **10**, 3208 (2019).
35. D. Wei, C. Wang, H. Wang, X. Hu, D. Wei, X. Fang, Y. Zhang, D. Wu, Y. Hu, J. Li, S. Zhu, and M. Xiao, Nat. Photonics **12**, 596 (2018).
36. D. Wei, C. Wang, X. Xu, H. Wang, Y. Hu, P. Chen, J. Li, Y. Zhu, C. Xin, X. Hu, Y. Zhong, D. Wu, J. Chu, S. Zhu, and M. Xiao, Nat. Commun. **10**, 4193 (2019).
37. W. B. Gandrud, IEEE J. Quantum Electron. **7**, 132 (1971).
38. N. Matsumoto, T. Ando, T. Inoue, Y. Ohtake, and T. Hara, J. Opt. Soc. Am. A **25**, 1642 (2008).
39. M. M. Fejer, G. A. Magel, and E. Lim, Proc. SPIE **1148**, 213 (1990).